Northumbria Research Link

Northumbria
University
NEWCASTLE

UniversityLibrary

Critical flux-based membrane fouling control of forward osmosis: Behavior, sustainability, and reversibility

Thanh-Tin Nguyen, Seungho Kook, Chulmin Lee, Robert W. Field[*], In S. Kim[**]

Global Desalination Research Center (GDRC), School of Earth Sciences and Environmental Engineering, Gwangju Institute of Science and Technology, 123 Cheomdangwagi-ro, Buk-gu, Gwangju 61005, Korea

[*]Department of Engineering Science, University of Oxford, United Kingdom

[**] Corresponding author.

In S. Kim

Email: iskim@gist.ac.kr

Telephone: +82-62-715-2477

Fax: +82-62-715-2434

Abstract

Membrane fouling is closely related to the concept of critical flux. Therefore, a fouling control stategy for forward osmosis (FO) membranes that is based on the critical flux is necessary. This study systematically investigated the critical flux behavior of FO membranes (CTA and PA-TFC) in the short-term using a stepping method (draw solution (DS) concentration stepping). In addition, to test the reliability of this method, long-term experiments were conducted to evaluate the influences of operational critical flux on the fouling behavior (sustainable operation and fouling reversibility/irreversibility), thereby determining the critical flux for reversibility. Our results showed that the DS concentration stepping could be applied for critical flux determination in FO. Both membranes exhibited higher critical flux values for alginate fouling compared to other single foulants such as colloidal silica or gypsum. The values were 15.9 LMH for a cellulose triacetate membrane (CTA) and 20.5 LMH for the polyamide thin-film composite (PA-TFC). Whilst these values should be adequate in FO applications they were determined for single foulants. The presence of multispecies of foulants caused a significant decline in the critical flux values. This study found 5.4 LMH for the CTA membrane and 8.3 LMH for the PA-TFC membrane for the combined foulants of alginate + gypsum. This indicates that the critical flux behavior in FO was dependent on the foulant type and membrane type. Importantly, 98-100% restoration of water flux was achieved with the PA-TFC membrane at an operation either close to or below critical flux (i.e., in case of negligible fouling), except for the combination of alginate-combined colloidal silica. The critical fluxes for reversibility obtained in this study will aid the efficient operation of practical FO processes.

2

1. Introduction

Forward Osmosis (FO) is an osmotically driven membrane process in which water is transported from low osmotic pressure (feed solution) to high osmotic pressure (draw solution) across the semipermeable membrane through the action of a chemical potential gradient [1]. Hybrid FO processes have recently emerged as possible systems for the simultaneous treatment of impaired/reclaimed water and seawater for reuse [2] [3] [4] [5] since standalone FO process cannot economically achieve either water treatment or desalination of seawater. These hybrid processes can bring many advantages regarding the energy consumption and the water quality: i) decrease of desalinated energy cost because seawater is diluted before entering RO desalination, ii) reduction of the fouling propensity of the RO stage through pretreatment of impaired water; (iii) a multi-barrier protection is established to improve contaminant removal; thereby giving opportunity for safe and high-quality reuse of impaired water [5] [6] [7]. In detail, complex wastewater (i.e., raw sewage, primary effluent, secondary effluent, biologically treated wastewater effluent) can be directly pre-treated by FO process (i.e., pre-treated wastewater or pre-concentrated wastewater) and subsequently potable water can be produced by combining with a draw solute recovery process (i.e., reverse osmosis or membrane distillation) [8] [9]. Despite less impact of fouling compared to RO (i.e. due to the absence of hydraulic pressure) the performance and large-scale implementation of FO process can be significantly affected by fouling [10]. The fouling, or to be more precise, the flux decline occurring with an FO membrane is generally considered to be less severe than that with a RO membrane. This has been attributed by some to the absence of applied hydraulic pressure; the foulant layer on a FO membrane is said to be looser whereas that on an RO membrane is said to be more densely compacted [11]. On the other hand others have found no difference in flux decline between FO and RO fouling, and attributed this to the low starting flux which was said to be below the critical flux [12]. Others have specifically suggested that foulant layer compaction

is physically related to water flux not hydraulic pressure [13] ADD [new ref]. Three major types of fouling occur in the FO membrane: (1) organic fouling caused by macromolecular organic compounds as polysaccharides, protein, and humic acid; (2) inorganic fouling involving the scaling with the crystallization of sparingly soluble mineral salts and colloidal fouling with the deposition of particles; (3) biofouling from bacteria attachment [14].

Membrane fouling is closely related to the concept of the critical flux, which was originally introduced by several authors [15] [16] [17], who reported: "below the critical flux, fouling occurs insignificant, whereas, above the critical flux, fouling becomes more severed". Therefore, the critical flux concept has been widely introduced to the full range of pressure-driven membrane processes, including microfiltration (MF) [18], ultrafiltration (UF) [19] [20], nanofiltration (NF) [21] [22] and even in RO [23] [24], to control fouling in desalination and water treatment processes. An operation below a critical value, called critical flux (where the distinction is between no fouling and fouling) or threshold flux (where the distinction is between low fouling and more extensive fouling) is favorable to the control of membrane fouling and thus the maintenance ofsustainable operation [25]. Membrane fouling comprises reversible and irreversible fouling, the difference being based on the degree of attachment of foulants to the membrane surface. This is a vital assessment to quantify the fouling propensity as well as the potential recovery of water flux. A sufficient shear force (i.e., physical flushing) can be used for the removal of reversible fouling but this is not the case with irreversible fouling. Numerous authors have investigated the fouling reversibility of FO under various scenarios: single fouling (i.e., alginate [26] [27], colloidal silica [26] [27], gypsum scaling [14] [28] [29], combined fouling (i.e., alginate + colloidal silica [27], alginate + gypsum scaling [14]), different membrane types [28] [30], and operating condition (i.e., effect of applied hydraulic pressure [27] [31]). Their results indicated that a higher restoration of

4

water flux is obtained with single foulants. Nevertheless, the effect of various initial fluxes (achieved by varying DS concentration) on the fouling reversibility has not been fully explored yet. The critical flux for reversibility has previously been introduced for pressure-driven process; efficiency and economical operation are favoured by operation below this value [32]. Thus, this concept is also expected to be applicable in FO membrane processes. To determine the critical flux, several methods can be used: flux–pressure profile, flux stepping, flux cycling, mass balance, and fouling rate analysis [32]. In particular, the stepping method is commonly used in pressure-driven membrane processes for critical flux determination, in which either the transmembrane pressure (TMP) or the flux is increased stepwise, and the response (either flux or TMP) is observed [32] [33].

Nevertheless, hitherto, little attention has been directed to the role of the critical flux of osmotically driven processes (FO) in controlling membrane fouling compared to that of pressure-driven processes (RO, NF, and UF). For instance, several authors have investigated the critical flux governing the fouling in the FO membrane through observations and experiments (Table 1) [34] [35] [36]. These studies have not systematically investigated the various fouling scenarios essential for applications such as the simultaneous treatment of impaired water for reuse and seawater desalination. In addition, past studies have focused on studying the commercial membranes principally those with low tomoderate permeability from HTI (i.e. their, cellulose triacetate (CTA) and thin film composite (TFC)). However, a newly developed polyamide thin-film composite (PA-TFC) from the Toray company was recently introduced as a potential candidate for the practical application due to its high permeability [37] [38] [39]. Therefore, a comparison of critical flux behavior between the former and latter membrane is essential to aid membrane selection. Moreover, as aforementioned, critical flux for reversibility is definitely beneficial but previous

studies (Table 1) have not performed the essential long-term evaluation. Therefore our work included a systematic study on the critical flux behavior in longer term operation whilst also comparing: CTA from HTI Company with PA-TFC membrane from Toray Company.

As mentioned above the stepping method is well known for the characterization of critical flux in pressure-driven processes. This was adapted for the current study. Instead of using pressure stepping (or flux stepping), the draw solution (DS) concentration stepping method (0.25–3 M) was used for the critical flux determination in various FO fouling scenarios under the short-term test. Moreover, to test the reliability of the DS concentration stepping method in this study, an essential investigation of the sustainability of the water fluxes was also performed in a series of long-term tests. These were run to determine membrane fouling behavior above the determined value of critical flux, at critical flux, and below critical flux. Additionally, in the current study, to solve the gap of the previous studies as mentioned beforehand, an assessment of the fouling reversibility around critical flux conditions was also made in order to determine the critical flux for reversibility.

Table 1. Summary of previous studies related to critical flux in FO membranes

138

Test method	Application	Foulant	Membrane	Results	Reference
Fouling surface coverage using direct microscopic observation through the me	Membrane-based seawater desalination	Latex microparticles (3 µm)	Cellulose Triacetate (CTA) flat sheet membrane (HTI)	FO critical flux for latex filtration was approximately 28 LMH. AL-FS orientation more fouling resistant than AL-DS. Feed spacer was able to considerably enhance initial flux and critical flux in FO (> 52 LMH)	[34]
Stepping method: Flux stepping (concentration stepping)	Membrane-based microalgae filtration	Microalgae 100 mg/L	Cellulose Triacetate (CTA) flat sheet membrane (HTI)	FO critical flux was between 9.3 and 15.5 LMH. Stable flux can be obtained by operating below the critical flux. Fouling was more severe and less reversible due to the presence of divalent ions (Mg^{2+}). A higher critical flux of 21 LMH was obtained with spacers in the feed channel	[35]
Long-term test: Flux decline observation	Membrane-based seawater desalination	Humic acid: 200 mg/L Alginate: 200 mg/L	Cellulose triacetate (CTA), thin-film composite (TFC) FO membrane (HTI) and TFC FO (Porifera Inc.)	Low-fouling behavior observed in FO (AL-FS), while operating at lower permeation of 10 LMH.	[36]

139

140

141

2. Materials and methods

7

2.1. FO membranes and characterization

FO membranes used in the current study include the CTA membrane from Hydration Technologies Inc., USA and a PA-TFC membrane from Toray Chemical Korea Inc., Korea. The CTA membrane was fabricated from cellulose acetate embedded in a polyester woven mesh [14]. Meanwhile, the PA-TFC membrane consisted of a selective polyamide active layer formed by interfacial polymerization on top of a polysulfone porous substrate [39]. Prior to experimental use, the FO membranes were soaked in deionized (DI) water and stored at 4 °C. For the membrane characterization, a cross-section of the pristine membrane was used to determine its thickness and the membrane morphology was analyzed using a high-resolution field-emission gun scanning electron microscope (FE-SEM), LEO Ge- mini 1525 (Carl Zeiss). The contact angle, determined using the sessile drop approach (Kruss G10 goniometer, Kruss, Germany), was used to characterize the hydrophobicity/hydrophilicity. The roughness of the membranes was determined using atomic force microscopy (AFM). To measure the A, B and S parameters, this study followed the procedures of the previous works [38] [40]. In detail, water permeability (A) and solute permeability (B) were determined using a pressure-driven filtration unit whilst structural parameter (S) was defined using an osmosis-driven filtration unit. For the permeability test, a stable water flux was obtained after membrane compaction test (10 bar) using DI within 2 hours. Afterwards, under an applied hydraulic pressure of 10 bar with 2000 ppm NaCl solution, water and solute permeability were determined by measuring the mass of permeate and NaCl rejection. For osmosis-driven filtration unit, water flux was measured in FO mode with DI (feed solution) and NaCl solution as draw solution (with concentrations of 0.1, 0.2, 0.5 and 1.0 M). The S parameter was calculated from the data, the pre-determined A and B values, following the equations given in a previous study [40].

8

The specific properties of the membranes including water permeability (A), solute permeability (B), thickness, hydrophobicity/hydrophilicity, surface roughness, are detailedin Table 2. The average roughness of PA-TFC and CTA are 50.5 mm and 23.9 nm, respectively, suggesting that the PA-TFC membrane has a rougher active layer surface. The lower contact angle of the PA-TFC indicates a more hydrophilic surface.

Table 2. Specific membrane properties

Properties		CTA	PA-TFC
Membrane thickness (µm)		59.3 ± 24.0	91.4 ± 1.3
Average surface roughness (nm)	Active layer	23.9 ± 8.9	50.5 ± 2.2
	Support layer	11.1 ± 1.6	20.4 ± 3.4
Hydrophobicity (°)	Active layer	50.0 ± 2.4	40.3 ± 2.4
	Support layer	58.1 ± 0.3	48.4 ± 0.7
Water permeability (A) (LMH Bar^{-1})		0.821	8.818
Solute permeability (B) (m s^{-1})		1.672×10^{-7}	2.457×10^{-7}
Structure parameter (S) (µm)		477 ± 30	276 ± 13

2.2. Model foulants

The model foulants used for the fouling experiments consist of sodium alginate, colloidal silica, and gypsum scaling, which represent the primary constituents of the major inorganic and organic components in wastewater effluent or surface water. Sodium alginate was used as the organic foulant; it consists of polysaccharides, in the molecular weight range of 12–80 kDa and is negatively charged [41]. It was obtained in powder form from Sigma–Aldrich, USA. Prior to introducing it into the feed solution (FS), 2 g/L of the sodium alginate stock solution was prepared by completely dissolving the powder in DI water for 24 h before keeping it at 4 °C. Colloidal silica (Snowtex ST-ZL) supplied by Nissan Chemical Industries, Tokyo, Japan, was used to represent the suspended colloidal matter. An average particle size of 139 nm was detailed by Bo et al. [42], for a colloidal suspension containing 40% w/w amorphous silica and 60% w/w water. The colloidal silica was stirred for 1 h to achieve complete dispersion before its use in the feed solution. With

185 regard to gypsum scaling experiments, stock solutions of 1 M $CaCl_2$ and 1 M Na_2SO_4, were

186 vigorously mixed for 24 h and then kept at 4 °C.

187

2.3. Feed and draw solutions

189 The FS used contained 10-mM NaCl for the baseline experiment and the fouling experiments. The

190 concentration of foulants in the feed solution was fixed at 200 mg/L and 1,000 mg/L for alginate

191 and silica, respectively whilst gypsum scaling was formed from 20-mM Na_2SO_4 and 20-mM $CaCl_2$.

192 The foulant concentrations were introduced either for single fouling or mixed fouling. To avoid the

193 effect a changes in the total ionic strength (IS) on flux behavior, the total IS was maintained at 0.13

194 M . To achieve this in the short-term operation (section 2.5) a fresh feed solution was prepared for

195 each step of DS concentration.. In brief, the detailed compositions of the FS for the baseline

196 experiment and fouling experiments are listed in Table 3. The FS pH was retained at 7.05 ± 0.03

197 using either 0.1-M NaOH solution or 0.5-M HCl solution. The concentration range of the NaCl DS

198 (0.25–3 M) was adjusted based on the experimental protocol of the short-term critical flux

199 determination experiment (described in detail in section 2.5).

200 **Table 3.** Components of feed solution for baseline and fouling experiments

Foulants	NaCl (mM)	Silica colloid (mg/L)	Alginate (mg/L)	Na_2SO_4 (mM)	$CaCl_2$ (mM)	IS Total (M)
Baseline experiment	10	0	0	40	0	0.13
Alginate	10	0	200	40	0	0.13
Colloidal silica	10	1000	0	40	0	0.13
Gypsum	10	0	0	20	20	0.13
Alginate + Colloidal silica	10	1000	200	40	0	0.13
Alginate + Gypsum	10	0	200	20	20	0.13

201 IS: Ionic Strength

202 **2.4. Lab-scale FO system setup**

203 Fig. 1 shows a schematic diagram of the lab-scale FO system. The system was operated in the

204 cross-flow mode for all experiments. An acrylic FO cell consisting of two rectangular channels

205 with dimensions of 75 mm (length) × 25 mm (width) × 3 mm (height) and an effective filtration

206 area of 1875 mm^2, was used to evaluate water permeation. No spacer was used for both the feed

207 and draw channels of the FO cell. A similar cross-flow velocity (CFV) of 6.66 cm/s using flow

208 meters was maintained in both the feed and draw channels. Circulation in counter-current mode

209 was maintained using a magnetic drive gear pump (GAF-T23-DEMSE MICROPUMP Inc., USA).

210 For the physical cleaning experiment, a high CFV of 13.32 cm/s was imposed on the feed side for

211 30 min with DI water. Additionally, to check the maintenance of the FO mode, pressure gauges

212 were installed in the DS and FS channels. The temperature was maintained at 23±1 $^\circ$C for the FS

213 and DS using a water bath. An electronic mass balance (GF-6100, A&D Company, Japan) was

214 used to record the variation in the DS mass to enable the calculation of the water flux.
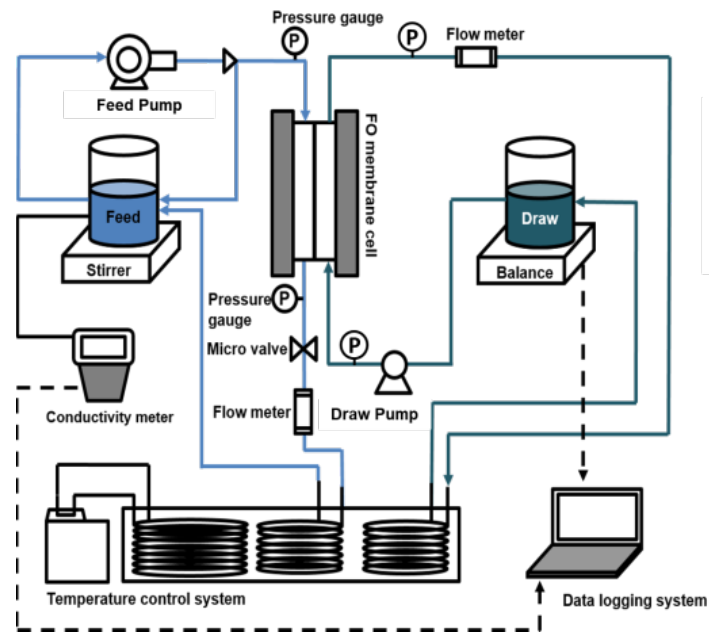
215

216 **Figure 1.** Schematic diagram of lab-scale FO system

217 **2.5. Short-term critical flux determination experiment**

218   For a typical critical-flux determination experiment, a membrane was placed in the test cell and

219   CFV adjustments of the DS and FS were made to reach the desired value of 6.66 cm/s. The DS and

220   FS were prepared with the same volume of 2 L. A stabilization testing for 30 min was performed

221   using DI water for both the FS and DS sides prior to the stepping experiments. Then DS

222   concentrations of 0.25-, 0.5-, 1.0-, 1.5-, 2.0-, and 3.0-M NaCl were employed consecutively to

223   conduct the DS concentration stepping method. Each test included the baseline stage (without

224   foulant) followed by the fouling stage. A difference between the two stages was the presence of

225   foulants in the FS in the latter stage. To avoid the influence of excessive DS dilution and FS

226   concentration, which may change the osmotic pressure, a stepping duration of 30 min was selected

227   from the study of Zou et al. [43]. Consequently, in every minute only 0.17–0.68 mL (CTA

228   membrane) and 0.29–1.26 mL (PA-TFC membrane) with respect to the DS concentration of 0.25–

229   3 M was permeated into 2 L of the DS; therefore such weak dilutions have a negligible effect. A

230   membrane orientation with the active layer facing the FS (AL-FS) was applied throughout all tests.

231

232   **2.6. Long-term FO fouling experiment**

233   To check the reliability of the DS concentration stepping method for the critical-flux determination

234   in the FO membrane, a long-term experiment was conducted to evaluate the influences of

235   operational critical flux on the fouling behavior including fouling reversibility/irreversibility. From

236   the critical flux value determined from the short-term experiments, operations above value, at this

237   value, and below this value were investigated for various fouling scenarios for both the CTA and

238   PA-TFC membranes (Table S-1). Similar to the short-term test, a FO test using DI water on both

239   the DS and FS sides was conducted to stabilize the system for the 30 min prior to the baseline

240   experiments. As FO flux reduction may also be influenced by factors other than fouling, such as

241   the dilution of the DS, which occurs in the AL-FS of an FO membrane [44], the baseline tests

242 (where foulant was absent) were also performed as a control test. The fouling experiments were

243 conducted by maintaining identical conditions of CFV, pH, and temperature corresponding to the

244 baseline tests. In the presence of a foulant, a water flux decline was observed. This is primarily due

245 to two factors: lower osmotic pressure due to dilution of DS and concentration of FS, and fouling

246 [44]. The extent of fouling could be evaluated by comparing the water flux curve of a fouled

247 membrane to the baseline which had similarly been influenced by dilution of DS and concentration

248 of FS. For every foulant, the length of the tests was 10 h. A physical cleaning test (water flushing)

249 was immediately performed for 30 min with an increased CFV value (as mentioned in section 2.3)

250 prior to repeating a baseline experiment with a reduction to the initial CFV. Subsequently, flux

251 recovery of the membrane was systematically evaluated to check for fouling reversibility, thereby

252 enabling a determination of the critical flux for irreversibility. During the physical cleaning

253 process, the feed was DI water, and the DS channel drained to ensure the absence of permeate flux

254 through the membrane.

255

256 **2.7. Parameter determination**

257 **2.7.1. Water flux**

258 In brief, the water flux was calculated based on the volume changes in the permeate as a function

259 of time (mintue by minute), which was adopted from the prior studies. The equation for water flux

260 is as follows:

261

262 $$J_t = \frac{1}{A_m}\frac{\Delta V}{\Delta t}$$ (1)

263

264 where J_t is the water flux (LMH) at time t, A_m is the effective membrane area (m^2, 0.001875 m^2 in

265 the current study), V is the volume of collected permeate (L), and t is the time for collecting the

266 permeate (h).

267

268 **2.7.2. Quantification of water flux decline for long-term experiments**

269 To evaluate the water flux decline caused by the effect of dilution or fouling, the percentage of flux

270 decline was considered to access the long-term operation. In the baseline experiment, a water flux

271 decline due to the effect of concentrating the FS and DS dilutions [44], which led to the loss of

272 osmotic driving force across the membrane is presented as follows:

273 % flux decline in baseline test= $(1- J_{wb}/J_{wbo})$ x 100% (2)

274

275 where J_{wb}/J_{wbo} is a normalized flux of the baseline experiment; J_{wb} is the final flux of the baseline

276 experiment (LMH); J_{wbo} is the initial flux of baseline experiment (LMH).

277 Meanwhile, a flux decline was induced simultaneously by the effect of dilution and the occurrence

278 of fouling in the fouling experiment:

279

280 % flux decline in fouling test= $(1- J_{wf}/J_{wfo})$ x 100% (3)

281 where J_{wf}/J_{wfo}, is a normalized flux of the fouling experiment; J_{wf} is the final flux of the fouling

282 experiment (LMH); J_{wfo} is the initial flux of the fouling experiment (LMH)

283

284

285

286 **2.7.3. Fouling reversibility**

287 The reversibility of the fouling layer deposited on an active layer was determined using physical

288 cleaning for 30 min with elevated CFV (twice the value used in the fouling experiment). The

289 cleaning effectiveness is shown in the equation below:

$$R\ (\%) = \frac{J_c - J_a}{J_b - J_a} \times 100 \tag{4}$$

291 where J_a is the water flux after the fouling experiment (LMH); J_b is the water flux before fouling

292 (pristine membrane) (LMH); J_c is the water flux after physical cleaning (LMH).

293

3. Results and discussion

3.1. Critical flux determination using single foulant

296 A comparison of the results from the baseline tests with those from single fouling tests is shown in

297 Fig. 2. The DS concentration was gradually increased via stepping from 0.25 M to 3 M with a step

298 interval of 30 min. The results allowed the determination of the critical flux behavior for an FO

299 single foulant. Regarding the baseline experiments, the water flux increased as the DS

300 concentration (and hence the osmotic driving force) was increased. A stable flux was obtained in

301 the baseline tests at various DS concentrations (0.25–2 M) for both the CTA and PA-TFC

302 membranes. However for the 3-M DS, a slight water flux decline was observed under the baseline

303 condition due to the combination of FS concentration and DS dilution; both lead to a loss of osmotic

304 driving force across the membrane [44]. The water flux of PA-TFC is approximately two times

305 higher than that of the CTA membrane, as shown in Fig. 2, despite having the same DS

306 concentration. This is due to the PA-TFC membrane having a lower structural parameter and

307 contact angle, and a much higher 'A' parameter (see Table 2). Subsequently, foulants such as

308 alginate (200 mg/L), colloidal silica (1000 mg/L), and gypsum scaling (20 mM Na_2SO_4 and 20

309 mM $CaCl_2$) were added singularly into the FS. The variation of water flux upon fouling with single

310 foulants is presented in Fig. 2.

311
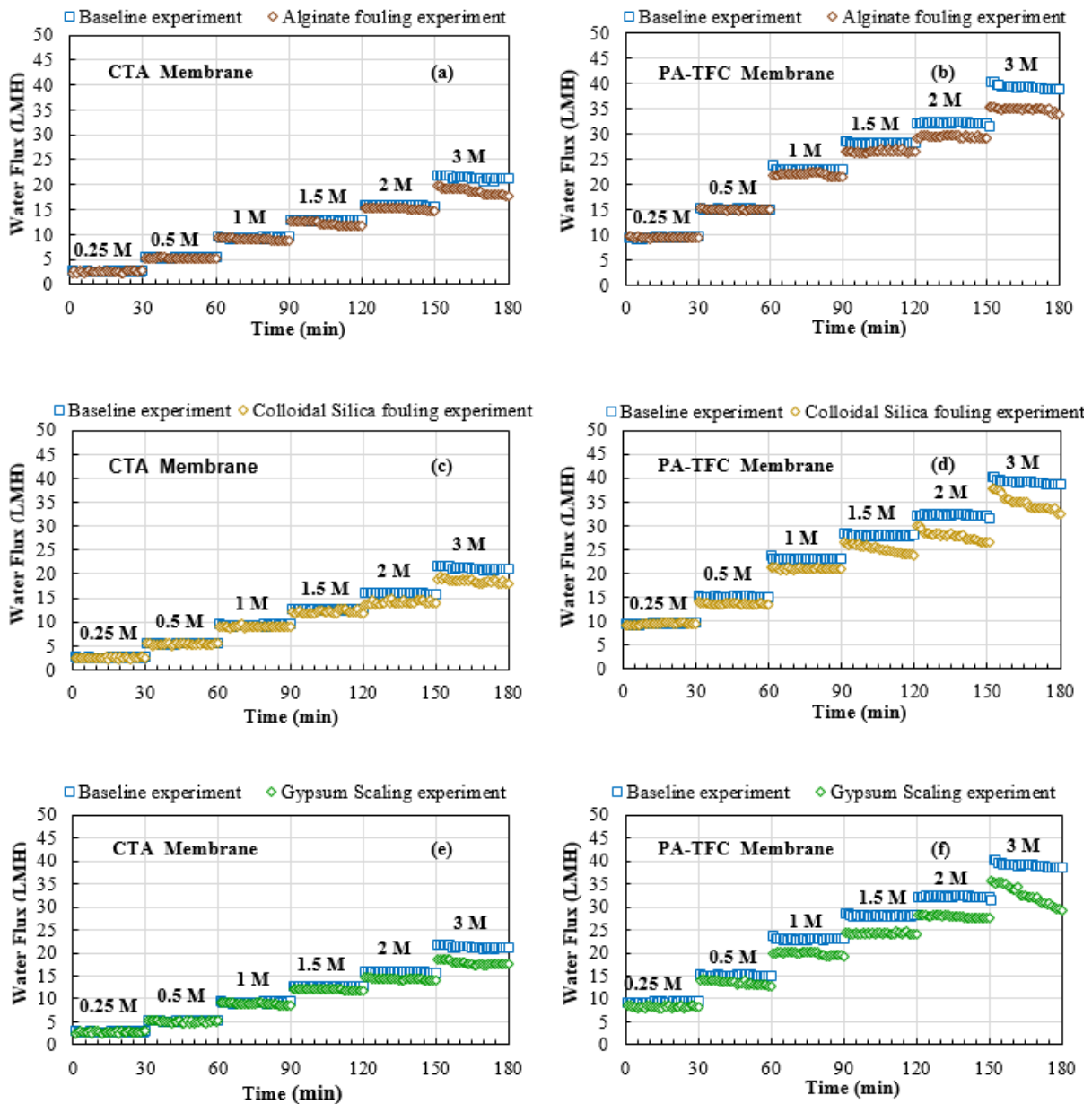
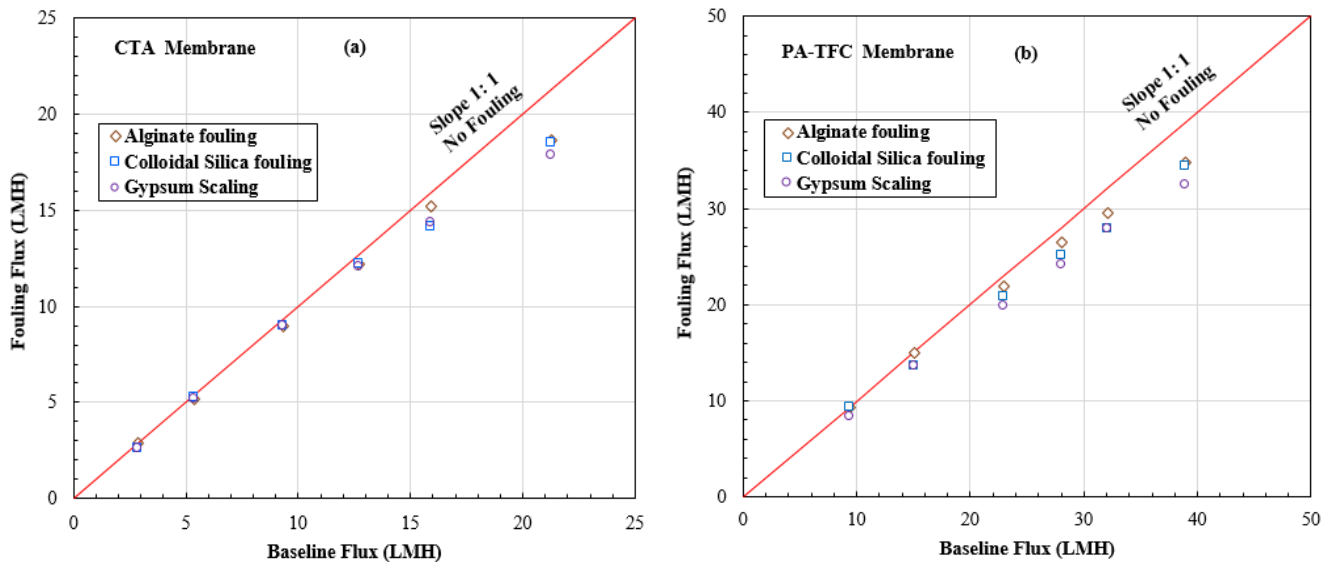**Figure 2.** Flux behavior of various single foulants: alginate (a, b), colloidal silica (c, d), gypsum

scaling (e, f), for a range of DS-concentrations (0.25−3 M) for the CTA membrane (left) and PA-

TFC membrane (right)

The degree of fouling can be evaluated by comparing the water flux curve of a fouled membrane

to the baseline. It is noteworthy that the fouling rate at various single fouling scenarios was

16

319   gradually promoted as the DS concentration is increased, corresponding to elevated water flux. The

320   increase in membrane fouling with a higher initial fluxcan be primarily attributed to the larger

321   hydrodynamic drag force that enhances the foulant deposition onto the membrane [46] [44] [47].

322   With respect to alginate fouling (Fig. 2-a, b), the flux curves overlap with the baseline flux curves

323   for DS concentrations of 0.25−1.5 M (flux: 2.7−12.5 LMH), and 0.25−0.5 M (flux: 8.3−12.8 LMH)

324   for the CTA and PA-TFC membranes, respectively. Otherwise, the water flux started deviating

325   from the baseline at higher DS concentrations of 2 M (CTA) and 1 M (PA-TFC), directly indicating

326   a reduction in water flux at these conditions due to the addition of alginate. In some cases the water

327   flux fouling flux did not decline although the initial flux in fouling was lower than that of the

328   baseline. This same trend was observed in a study by Zou et al., [43], who observed foulant

329   deposition onto a membrane using direct microscopic observation.

330

331   Fig. 2-c, d, e, f present the fouling trends of colloidal silica and of gypsum scaling with respect to

332   each DS concentration (0.25−3 M). Similarly, an overlap between the fouling flux and baseline

333   flux was observed for DS of 0.25−1.5 M for the CTA membrane, which shows the same trend as

334   alginate fouling. We can assume that the CTA membrane is less sensitive to various single foulants

335   when operating at a low or moderate initial flux. Meanwhile, for the PA-TFC membrane, this

336   overlap only appeared at a low DS of 0.25 M. A deviation from the baseline flux was immediately

337   recorded when operation at 1-M DS was started for both colloidal silica and gypsum scaling.

338   Specifically, a steady upward trend in fouling of the colloidal silica and gypsum was observed with

339   further increases in DS concentration. In particular the PA-TFC membrane was found to be more

340   prone to fouling by a single foulant at an operation of moderate or high initial flux (28.0−39.0

341   LMH). This agreed with the study of Yu et al. [49], who reported that severe fouling can occur

342   even at moderate flux levels (25 LMH), especially for PA-TFC. Additionally, they reported that

343　for TFC membranes the surface roughness plays a more dominant role over surface hydrophilicity

344　in membrane fouling [49]. Moreover, membrane surface morphology has been demonstrated as a

345　factor that largely affects the foulant–membrane interaction [48]. Therefore, with a much rougher

346　surface (data in Table 2) and a higher initial flux (Fig. 1), the fouling by a single foulant in the PA-

347　TFC membrane can be more significant, for a given DS concentration, compared to that with the

348　CTA membrane. This result is also consistent with that of Mazlan et al. [30], who indicated a

349　greater adhesion of foulant on the TFC active surface, which could be attributed to factors such as

350　surface roughness, surface charge, surface chemical heterogeneity, and hydrodynamic effects.

351　Finally we note that for the same flux of say 15.0 LMH the rate of fouling was similar for both

352　membranes.

353

354　**Figure 3.** Critical flux behaviors when various single foulants (◊) alginate, (□) colloidal silica, and

355　(○) gypsum scaling) were tested in AL-FS orientation for (a) CTA membrane and (b) PA-TFC

356　membrane. The fouling flux was plotted against the baseline flux, and data points below the line

357　with 1:1 slope indicate the occurrence of flux decline due to fouling.

358

359 Based on the flux measurements, a precise determination of the critical flux values was made by

360 plotting the fouling flux (at the end of each DS concentration step) against the corresponding

361 baseline flux (Fig. 3). The line with a 1:1 slope denotes no fouling (i.e., fouling flux equals the

362 corresponding baseline flux). Each foulant type has specific properties (i.e., alginate: transparent

363 gel layer [31], colloidal silica: particulate [26] [50], gypsum: crystallization [51]), thus resulting in

364 various forms of membrane interactions, leading to different fouling potentials on the FO

365 membrane. When the FS contains only a single foulant, a mild fouling condition is induced but

366 with a strong membrane dependence [49]. Membrane surface properties (surface roughness, caused

367 by functional groups bonding) and hydrodynamic conditions (initial flux, cross-flow velocity) have

368 been known to be vital factors for controlling membrane fouling [30]. Therefore, a distinct critical

369 flux behavior between CTA and PA-TFC can be anticipated. As illustrated in Fig. 3-a, the critical

370 flux behavior of the CTA membrane for alginate fouling was found to be within the range of 12.5−

371 15.9 LMH (critical DS 1.5−2 M). A critical flux value of 12.5 LMH (critical DS 1.5 M) was found

372 for both the colloidal silica and gypsum scaling. Regarding PA-TFC, a higher critical flux was

373 found for alginate compared to the other foulants, the value being 20.5 LMH (critical DS 1 M)

374 compared to 12.8 LMH (critical DS 0.5 M). Interestingly, the critical flux values by the single

375 foulants were higher for the PA-TFC membrane compared to those of the CTA membrane although

376 previous studies have reported that PA-TFC has a more pronounced fouling propensity [49] [48]

377 [30]. As noted in [32], the length of experiments can influence the determination of the critical

378 flux values. Thus to refine the determination of critical values, an essential investigation into

379 operational critical fluxes with long-term experiments was performed (in section 3.3.1).

380

381 **3.2. Critical flux determination using combined foulant**
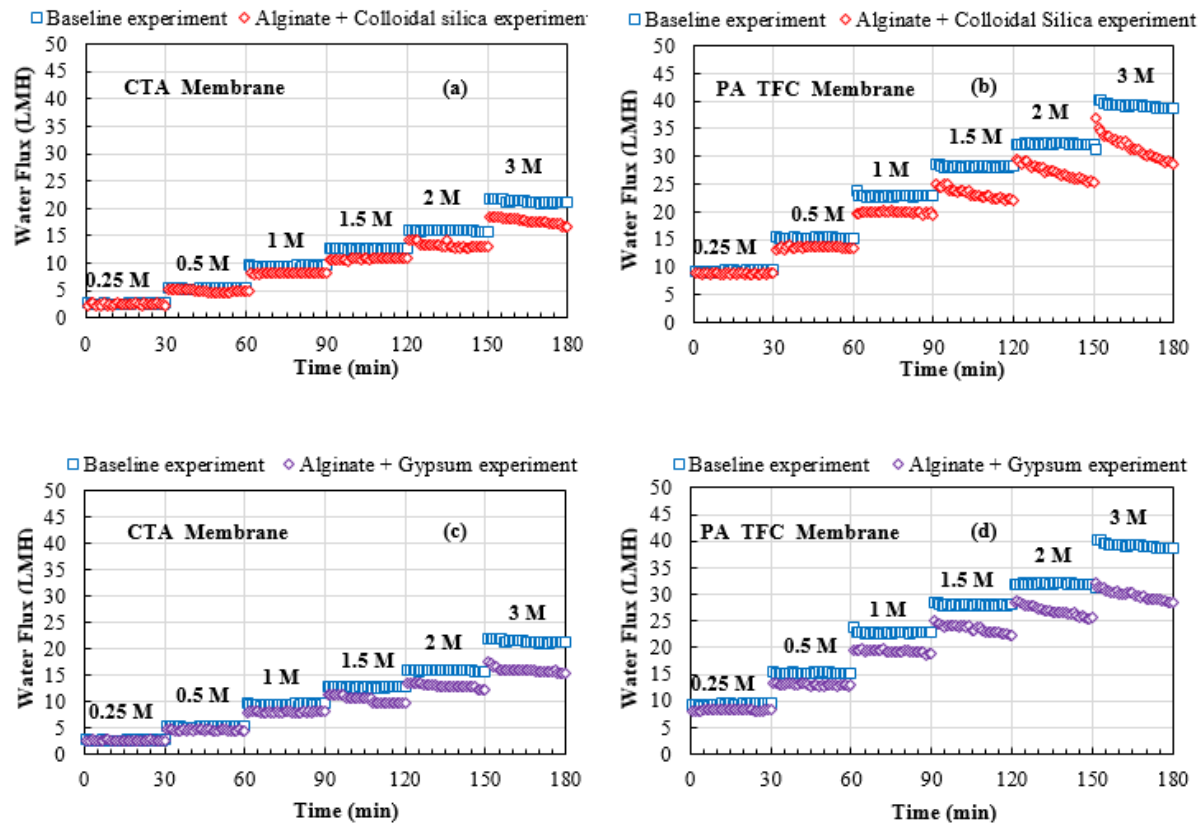
Figure 4. Flux behavior of various combined foulants (a, b) alginate + colloidal silica, (c, d) alginate + gypsum scaling with the DS-concentration step function (0.25−3 M) for CTA membrane (left) and PA-TFC membrane (right)

In general, various foulant types are present in wastewater and surface water. Therefore an investigation of the critical flux behavior by combined fouling is necessary. Fig. 4 presents the flux behavior of various combined foulants (i.e., alginate + colloidal silica, and alginate + gypsum scaling) as the DS-concentration is increased step wise from 0.25 to 3 M both for CTA membrane (a, c) and PA-TFC membrane (b, d). Regarding the CTA membrane, at low DS concentrations of 0.25−0.5 M (corresponding to low flux of 2.7−5.4 LMH), an entire overlap between the fouling flux and baseline flux was observed for the combined foulants (Fig. 4-a, c), indicating negligible fouling. In contrast, at DS concentrations of 1−3 M (flux range 9.0−17.8 LMH), fouling started to

20

395   appear as indicated by the fouling flux deviating from the baseline flux. This indicates that for the

396   CTA membrane an effective control of combined fouling can only be achieved at an extremely low

397   initial flux, which might be insufficient for economical application of FO membrane process.

398

399   For the PA-TFC membrane, only DS of 0.25 M (corresponding to flux of 9.4 LMH) showed an

400   overlap between the fouling flux and baseline flux (i.e., negligible fouling). When the DS was

401   increased from 0.5 M to 3 M, fluxes in the range 12.8−39.0 LMH were found but there was

402   deviation between the fouling flux and the baseline flux for DS concentration of 0.5 M upwards.

403   The extent of fouling increased steadily with increased DS concentration. From Fig. 4, for each DS

404   concentration it can be observed that clear deviation follows the following order: alginate + gypsum

405   > alginate + colloidal silica. Also PA-TFC > CTA and the reasons for this are primarily due to the

406   higher initial flux [26] [50] [51] and rougher surface of the PA-TFC membrane (Table 2). The

407   finding of a more complex fouling by alginate combined with gypsum accords with those of others

408   [14] [49] [52]. Gu et al. [49] reported that severe fouling for PA-TFC at either moderate flux levels

409   of around 25.0 LMH or with combined foulants. They mentioned that in addition to membrane−

410   foulant interaction, foulant−foulant interaction was important [49]. Moreover and more generally,

411   previous studies have reported that a susceptibility to fouling occurs when the membrane surface

412   becomes covered by fouling [44] [49] [52]. Consequently, further deposition is governed by

413   interaction between the foulant cake layer and foulants in the FS [49].

414
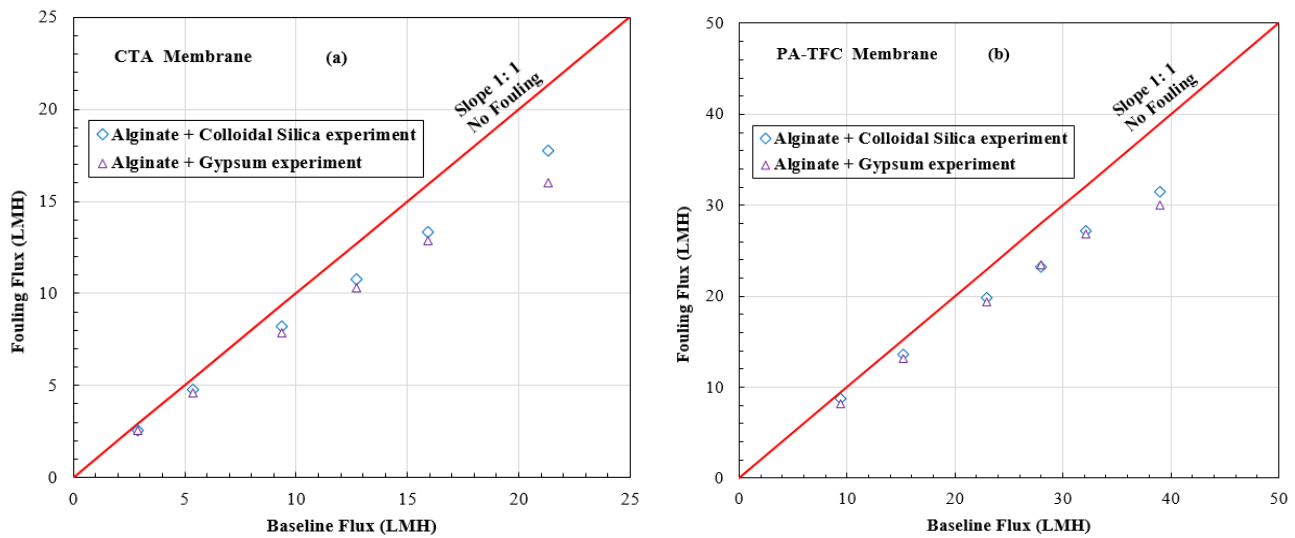
Figure 5. Critical flux behaviors when various combinations of foulants: (◊) alginate + colloidal silica, (Δ) alginate + gypsum scaling were tested in the AL-FS orientation for (a) CTA membrane and (b) PA-TFC membrane. The fouling flux was plotted against the baseline flux, and data points below the line with 1:1 slope indicate the occurrence of flux decline due to fouling.

As illustrated in Fig. 5, the fouling flux is plotted against the corresponding baseline flux to determine the critical flux values for combined foulants. As mentioned above (section 3.1), the potential fouling on an FO membrane was different for each foulant type. However, when more than one type of foulant is present, the interaction among foulants can result in various changes such as physical changes in size and molecular weight and chemical changes e.g. charge and hydrophobicity [53] [41] [51] [52] [54]. Such changes explain the finding that the critical flux for the CTA membrane was just 5.2 LMH (corresponding to DS 0.5 M) for both combined fouling conditions. This value is to be compared to the finding that for single foulants the critical flux was between 12.5 and 15.9 LMH. The determination of the critical flux behavior of PA-TFC membranes under combined fouling conditions found that for alginate combined with colloidal

22

431 silica the critical flux was 12.8 LMH (corresponding to DS 0.5 M). Meanwhile, for alginate +

432 gypsum the value is lower than 9.4 LMH (corresponding to DS < 0.25 M). Whilst a short-term test

433 at a lower DS concentration was not performed, a DS concentration of 0.15 M was investigated in

434 long-term test of alginate + gypsum fouling (in section 3.3.2)

435

436 **3.3. Membrane fouling behavior in long-term tests**

437 **3.3.1 Single foulant**
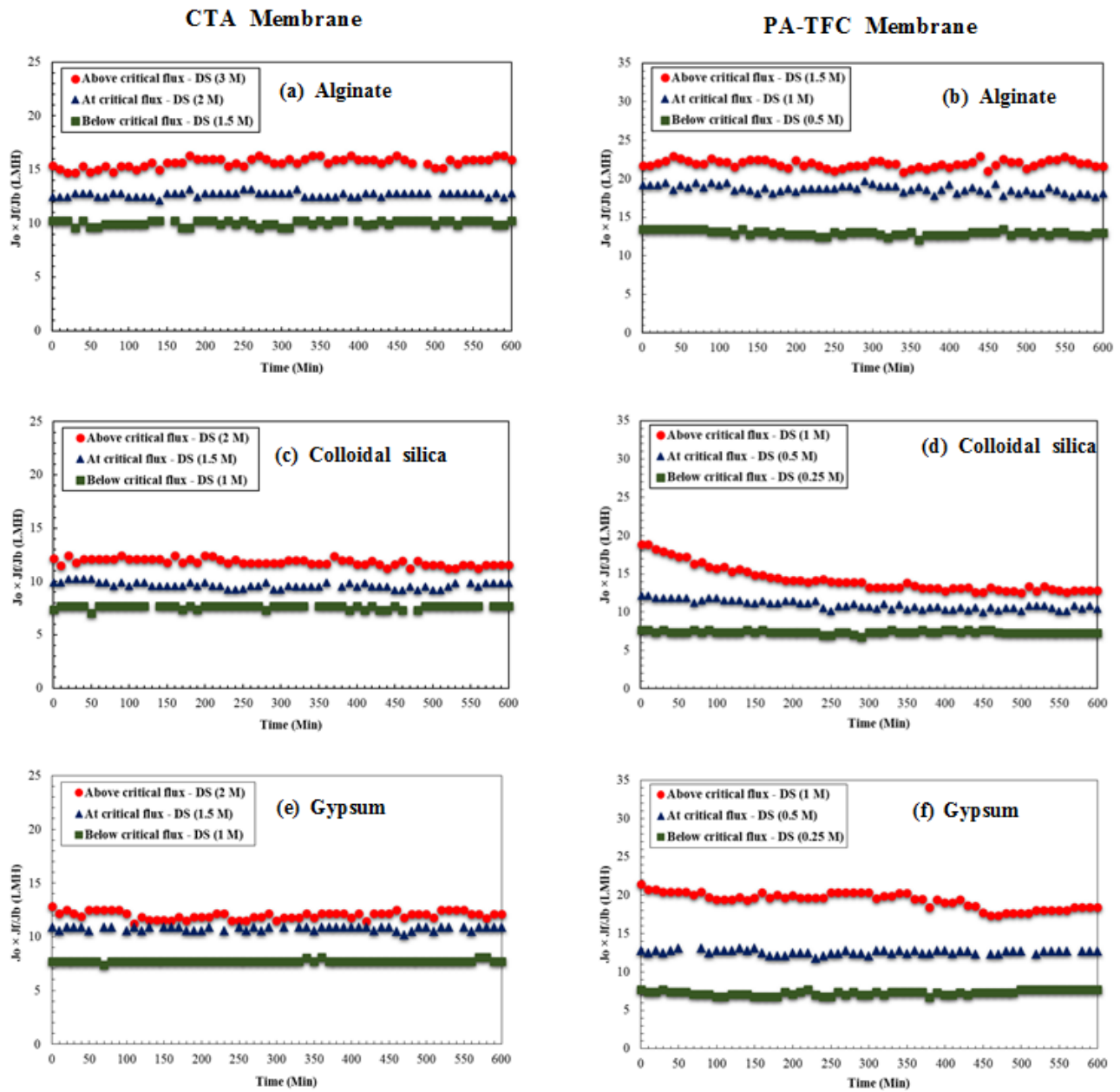
Figure 6. Water flux behavior as a function of time for various single foulants under three operational conditions: above critical flux, at critical flux, and below critical flux. Single fouling experiments:(a, b) alginate, (c, d) colloidal silica, (e, f) gypsum scaling for CTA membrane (left) and PA-TFC membrane (right). $J_o \times J_f/J_b$ is a normalized representation of the extent of membrane fouling. J_o represents the initial flux, J_f is the flux in the fouling test, J_b is the baseline flux.

444 According to the critical flux value obtained in the short-term test (in section 3.1), a long-term

445 experiment of 10 h was performed to not only investigate the reliability of the DS concentration

446 stepping method but also to determine the influence of the fluxes around these critical values on

447 the fouling behavior. Fig. 6 shows the water flux decline as a function of time at various single

448 foulants under operational critical fluxes (above critical flux, at critical flux, below critical flux).

449 The desired DS concentration was changed based on the design shown in Table S-1. In the baseline

450 experiments for both membranes (Fig. S-2), water flux flows from the feed to the draw side,

451 inherently induces a simultaneous concentration of feed and dilution of the draw. A higher water

452 flux reduction was caused by the larger dilution [44], which became severe in the PA-TFC

453 membrane because of higher flux. For the CTA membrane, by comparing the water flux curve of

454 a fouled membrane to the baseline (J_o x J_f/J_b is a normalized representation of the extent of

455 membrane fouling), the extent of fouling could be evaluated for the various single foulants such as

456 alginate, colloidal, and gypsum (Fig. 6- a, c, e and Fig S-2-a, c, e). An unstable flux (Fig. 6) and a

457 flux reduction caused by fouling (Fig S-4) was observed above the critical flux, i.e., 3-M DS

458 (alginate), 2-M DS (colloidal silica), 2-M DS (gypsum), whereas negligible or even no fouling

459 occurred at the critical flux and below it. When operating below the critical flux, the flux decline

460 appears to result only from the effect of draw dilution (Fig. S-4), which indicates less sensitivity to

461 single fouling of the CTA membrane (as stated in section 3.1). These findings suggest the existence

462 of critical fluxes (J_{crit}) for single foulants and the CTA membrane as follows: $J_{crit} \approx 15.9$ LMH

463 (alginate), $J_{crit} \approx 12.5$ LMH (colloidal silica), $J_{crit} \approx 12.5$ LMH (gypsum). Obviously, a sustainable

464 operation without fouling could be achieved by setting an appropriate flux (i.e., close to or below

465 critical flux); this promotes the minimization of fouling of the CTA membrane by single foulants.

466

467 Regarding the PA-TFC membrane (Fig. 6-b, d, f and Fig S-2, b, d, f), fouling occurred above the

468 critical flux being considerable for colloidal silica, moderate for gypsum and slight for alginate,

469 with all being much greater compared to that with the CTA membrane. As mentioned in sections

470 3.1 and 3.2, either a high initial flux or the properties of the membrane surface (i.e., much rougher,

471 bonding of functional groups) was the primary reason of vulnerable fouling in the PA-TFC

472 membrane. This finding accords with others for instance, Mi et al. [55] demonstrated that surface

473 roughness caused an increase in the adhesion force between the PA-TFC membrane and a colloidal

474 silica gel layer. Kim et al. [56] also concluded that the structure of colloidal fouling was

475 significantly dependent on the initial permeate flux, with the fouling transitioning from fluid-like

476 to solid-like [57], thereby promoting excessive fouling [51]. According to previous studies, severe

477 fouling with colloidal silica is to be expected and for the resultant flux decline to be magnified by

478 the effect of cake enhanced-concentration polarization (CE-CP), thereby significantly increasing

479 the overall FO flux decline [42] [26] [50] [28]. Meanwhile, gypsum scaling was accelerated

480 because of a greater membrane surface roughness [58] [59] and the rich presence of the carboxylic

481 group (-COO-), which could interact with the Ca^{2+} ions to form a complex foulant [51] [59].

482 Additionally, the role of the initial flux was also pronounced in the gypsum scaling behavior, i.e.,

483 more than 50% water flux decline was recorded when the initial flux was increased from 10 LMH

484 to 25 LMH with PA-TFC [51]. Other previous studies have indicated that a dominant

485 heterogeneous crystallization occurs in gypsum scaling on PA-TFC, thus causing a much larger

486 degree of fouling than that with a CTA membrane [51] [29]. Fig. 6 and Fig. S-4 show that the

487 considerable flux decrease via fouling began to appear with colloidal silica foulant, when operating

488 above the critical flux condition. Contrastingly just a minor degree of fouling and a sustainable flux

489 were observed close to or below the critical values. When there is an acceptable minor degree of

490 fouling it has been suggested that the term threshold flux be used and it can be defined as the flux

26

at or below which low fouling occurs but above which the fouling rate increases significantly [25].

492 However this distinction is not made here. With single foulants and the PA-TFC membrane,

493 operation is super-critical at a higher flux of 20.0 LMH, but fouling control could be successfully

494 achieved by operation at the following values: $J_{crit} \approx 20.5$ LMH (alginate), $J_{crit} \approx 12.8$ LMH

495 (colloidal silica), $J_{crit} \approx 12.8$ LMH (gypsum).

496

497 **3.3.2 Combined foulant**

498 Fig. 7 depicts the water flux behavior as a function of time for various combined foulants under at

499 fluxes above critical flux, at critical flux, and below critical flux. The corresponding DS

500 concentrations are given in Table S-1. As discussed in section 3.2, the presence of colloidal silica

501 or gypsum partially contributed to the formation of a complex foulant layer, causing a more severe

502 fouling. For example, the study of Motsa et al. [41] demonstrated that the significant flux loss of

503 the CTA membrane in combined fouling (i.e., alginate + colloidal silica) was due to the hydraulic

504 resistance of a gel layer that hindered back diffusion of the colloid and gave rise to CE-CP. Their

505 experiments were operated with an initial flux of 15.8 LMH (i.e., DS 3.5 M). In addition, the

506 synergistic effect of combined fouling (i.e., alginate + gypsum) was investigated at an initial flux

507 of 17.6 LMH (DS 4 M), in which accelerated gypsum scaling due to CE-CP has been reported for

508 a CTA membrane [14]. Liu et al. [52] found that alginate molecules could act as nuclei for gypsum

509 crystal growth, thus considerably increasing the gypsum crystal size and aggravating their

510 deposition onto a CTA membrane; their experiments were operated with an initial flux of 16.2

511 LMH. However, in the current study with the CTA membrane, combined fouling (i.e., alginate +

512 gypsum) only a slight flux decline above the critical flux was observed. This is due to a lower initial

513 flux (operation was at 9.0 LMH corresponding to DS 1 M) and a lower Ca^{2+} concentration (i.e.,

514 20-mM Na_2SO_4 and 20-mM $CaCl_2$ was used in this study). In previous studies the initial fluxes

515 were 16.2–17.6 LMH and Ca^{2+} concentration was higher owing to the use of 20-mM Na_2SO_4 and

516 35-mM $CaCl_2$ [14] [52]. Meanwhile in the present study sustainable fluxes were found at the

517 critical flux and below the critical flux (i.e., DS 0.5 M and DS 0.25 M) (Fig. 7-a, c). Clearly with

518 respect to the CTA membrane, control of combined fouling can be achieved by selection of an

519 appropriate DS concentration; a lower DS concentration gives a lower initial flux.

520
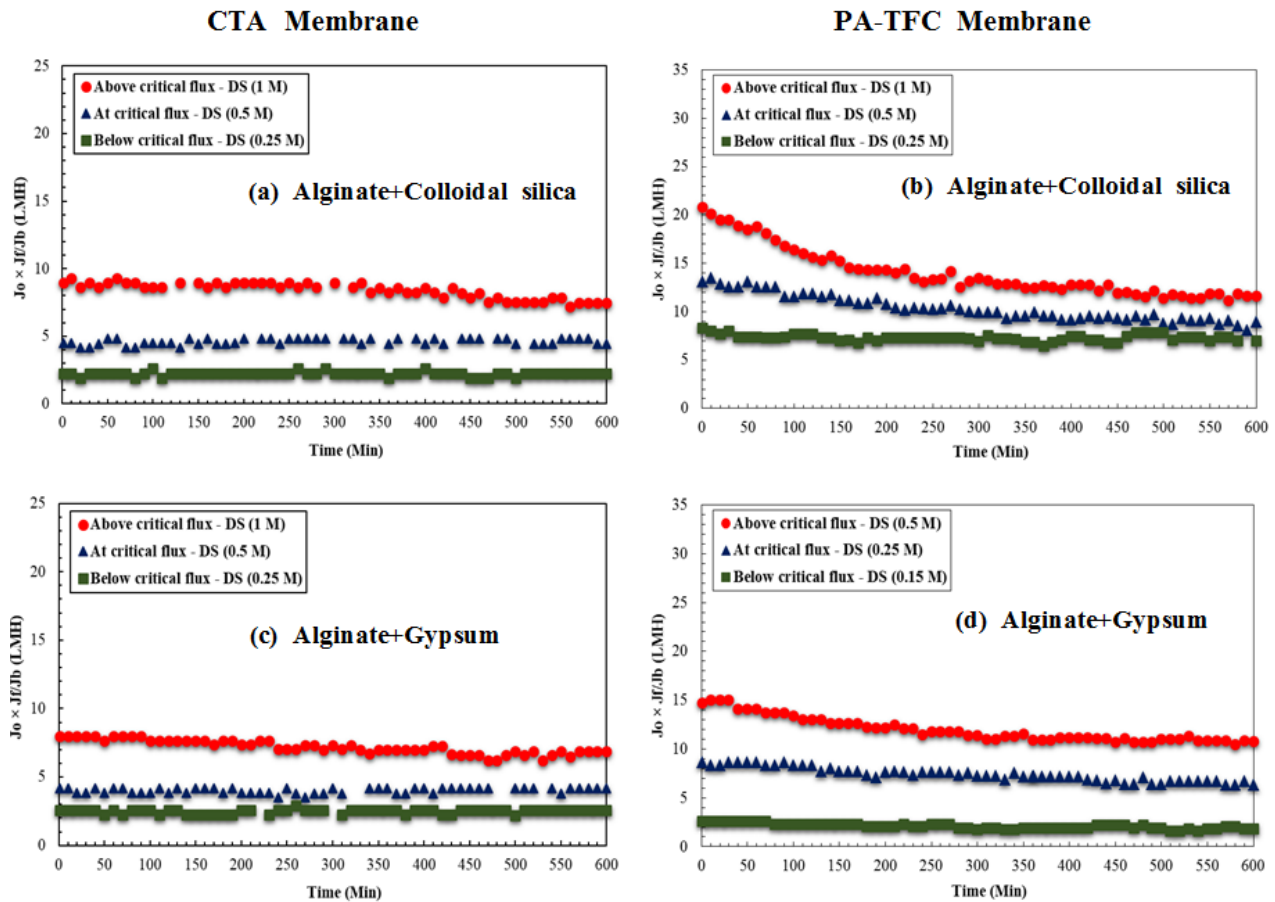
521

522 **Figure 7.** Water flux behavior as a function of time for combined foulants under three operational

523 conditions: above critical flux, at critical flux, and below critical flux. (a, b) alginate + colloidal

524 silica, (c, d) alginate + gypsum scaling for CTA membrane (left) and PA-TFC membrane (right).

525 $J_o \times J_f/J_b$ is a normalized representation of the extent of membrane fouling. J_o represents the initial

526 flux, J_f is the flux in the fouling test and J_b is the flux in the baseline test.

28

527

Above the critical flux the water flux declined dramatically after 10 h of operation, indicating

significant fouling (Fig. 7-b, d and Fig S-3-b, d). However, a negligible fouling of PA-TFC was

observed below the critical flux for both combinations of mixed foulants, resulting in a sustainable

flux. The critical flux values for the combined foulants were different being $J_{crit} \approx 12.8$ LMH for

alginate + colloidal silica and $J_{crit} \approx 8.3$ LMH for alginate + gypsum. Clearly, for the PA-TFC

membrane fouling control with alginate + gypsum is more difficult than that of alginate with

colloidal silica. As discussed in section 3.1, for single gypsum fouling, the presence of a rich

carboxylic group (-COO-) in PA-TFC [37] could interact with the Ca^{2+} ions to generate a

homogeneous crystallization [52]; this being an example of adverse membrane–foulant interaction.

Moreover, this fouling becomes more severe in the presence of alginate (i.e., a large number of

negatively charged carboxylate (-COO-)). A more complex matrix with the calcium ion of gypsum

is created which increases the crystal size[14]; this being an example of adverse foulant–foulant

interaction. A summary of critical flux values is given in Table 4.

541

542

543

544

545

546

547

548 **Table 4.** Critical flux values for fouling (LMH)

Foulants	Critical Flux for fouling (J_{crit})	
	CTA	PA-TFC

Single foulant		
Alginate	15.9	20.5
Colloidal silica	12.5	12.8
Gypsum	12.5	12.8
Combined foulants		
Alginate + gypsum	5.4	8.3
Alginate + colloidal silica	5.4	12.8

549 Note: The critical values above are specific for the FO membrane process with the conditions: i)

550 FO mode (AL-FS), ii) Feed and draw flow rate of 300 mL/min (equivalent CFV of 6.66 cm/s), iii)

551 Foulant concentration: 200 mg/L alginate, 1000 mg/L colloidal silica, gypsum scaling (20 mM

552 Na_2SO_4 and 20 mM $CaCl_2$) and iv) determination after flux stepping with a step interval of 30mins.

553

3.3.3 Fouling reversibility and critical flux for reversibility

555 Distinguishing between reversible and irreversible fouling is a vital to a proper assessment of the

556 fouling propensity of a FO membrane as well as to the potential recovery of water flux. Therefore,

557 in the current study when fouling had occurred, membrane flushing was performed for 30 min after

558 the fouling test to assess the degree of fouling reversibility . The results enabled us to establish the

559 critical flux for reversibility (J_{ci}). Fig. 8 shows the water flux recovered after the physical cleaning

560 of membranes fouled in the single foulant studies; there aresome blanks were the test was not

561 performed because there had been no fouling. In detail, the normalized flux after fouling showed

562 an increasing trend as the DS concentration decreased (i.e., lower initial flux), for both membranes

563 and three single foulants. As discussed in section 3.1, factors such as the initial flux, foulant type,

564 and membrane type led to a different impact on the membrane fouling propensity.

565

30

Regarding alginate fouling (Fig. 8-a), PA-TFC showed a higher fouling rate than the CTA membrane above critical flux conditions because of a higher initial flux. Nevertheless, we noticed that the flux recovered by physical cleaning appear to be the same for both membranes, with recoveries of 95%. It is likely that the fouling by alginate could be readily reversible, which was successfully demonstrated in previous studies with the CTA membrane [14] [31] [26] [27] and PA-TFC membrane [11]. Interestingly, 98-100% recovery of water flux was recorded at close to and below the critical flux i.e. 12.8 LMH (DS 0.5 M) for the PA-TFC membrane and at above critical flux i.e. 15.9 LMH (DS 3 M) for CTA membrane; thus, they do accord with the critical flux for reversibility [32]. As stated in section 3.1, although PA-TFC still exhibited a slight fouling with alginate below the critical flux (Fig. S-4, b), this fouling could be completely restored (Fig. 7-a). Obviously, an appropriate operation (i.e., close to or below critical flux) could help minimize the alginate fouling of PA-TFC membranes and promote fouling reversibility. A lower DS concentration was set to meet the operational critical flux conditions in colloidal silica fouling (Fig. 8-b). As mentioned in section 3.3.1, in operation above the critical flux, colloidal silica showed a more noticeable fouling tendency than alginate despite operation being at a lower initial flux (lower DS concentration) (Fig. 6). This was particularly noticeable with the PA-TFC membrane, which reached a low normalized flux of 0.55 after the formation of the fouling layer (Fig. 7-b). In addition, a low cleaning effectiveness was found for PA-TFC (i.e., 50%) indicating that with colloidal silica fouling this membrane gave poor recovery when starting above the critical flux (i.e., 20.5 LMH). This trend is consistent with the study of Xie et al. [53], who showed the effect of initial flux on the recovery of a TFC membrane subject to colloidal fouling (e.g., a flux of 20 LMH corresponded to a low recovery of 30%). However, for both membranes, a better recovery after colloidal silica fouling was obtained after operation at critical flux i.e. at 12.5 LMH (CTA) and 12.8 LMH (PA-TFC), and below critical flux condition i.e. at 8.3 LMH (PA-TFC). For the former and latter, high

values of 94% and 100% recovery respectively were found (Fig. 7-b). The study of Mi et al. [55] indicated that the surface roughness of PA-TFC played an important role in increasing the membrane–silica interaction, thus significantly decreasing the water flux recovery. However, in this study, it is noteworthy that PA-TFC exhibited a completely reversible fouling (roughly 100% recovery) when operating below the critical flux i.e., at 8.3 LMH (DS 0.25 M). Regarding gypsum scaling, it can be remarked that the physical cleaning appears to be more efficient after gypsum fouling of the CTA membrane with a high value of 97% recovery for operation above critical flux i.e. 15.9 LMH (DS 2.0 M). For the PA-TFC membrane similar recovery (98%) was found at the critical flux condition i.e. 12.8 LMH (DS 0.5 M). In summary, after fouling with single foulants membrane permeability could be well recovered by simple physical cleaning. Consequently this mode may offer the extraordinary advantage of significantly reducing or even eliminating chemical cleaning. The concept of critical flux for reversibility (J_{ci}) was defined by Bachin et al. [34] as "the permeate flux above which a multi-layer of irreversible fouling occurs". This accords with the results above and thus shows the existence of a critical flux for reversibility for both FO membranes tested. The J_{ci} results for the CTA and PA-TFC membranes are summarised in Table 5.
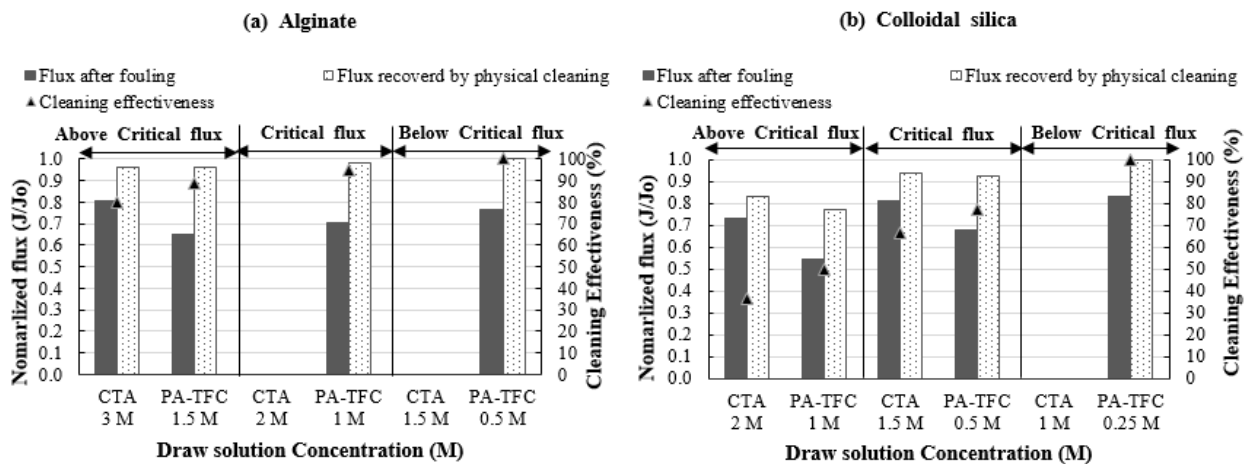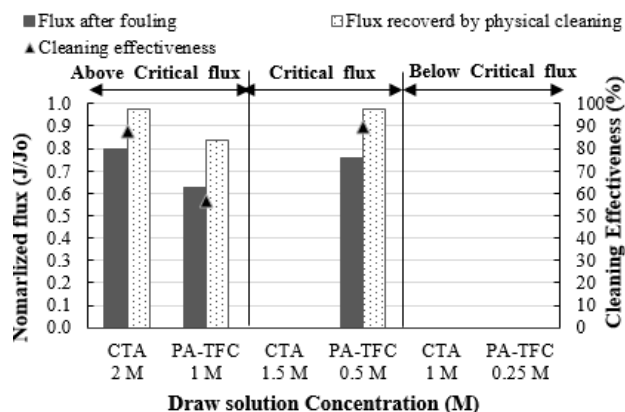
(c) Gypsum
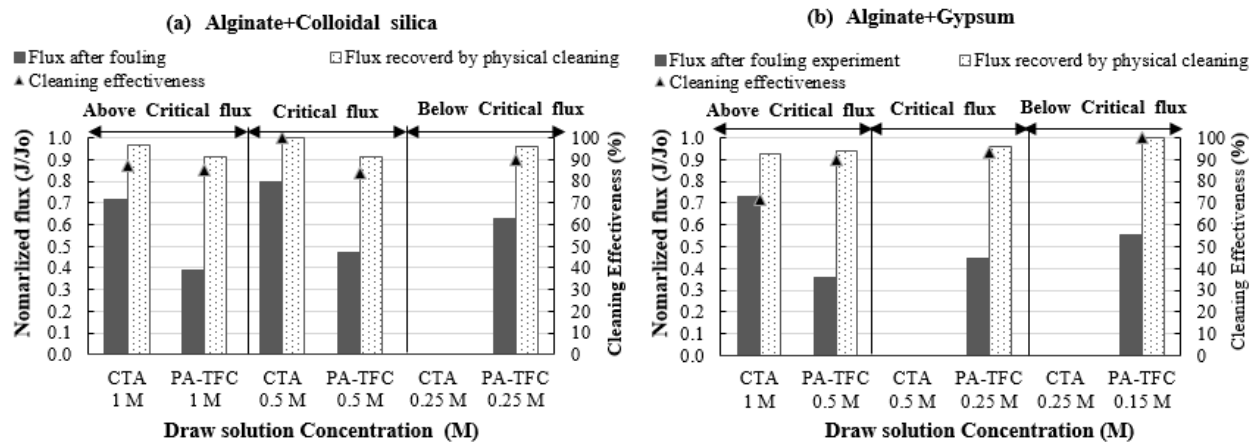
Figure 8. Water flux recovery after physical cleaning of membranes fouled by various single foulants: (a) alginate, (b) colloidal silica, (c) gypsum scaling at various operational fluxes (above critical flux, critical flux, below critical flux). Flux recovery was calculated from water permeability measuremnts taken between 15 min and 30 min after the physical cleaning step. Blanks exist where no fouling was observed during the fouling tests. (Alginate: CTA- DS 2M (at critical flux), 1.5 M (below critical flux); Colloidal silica: CTA-DS 1M (below critical flux); Gypsum: CTA- DS 1.5M (at critical flux), 1M (below critical flux) and PA-TFC- DS 0.25 M (below critical flux)).

An investigation of fouling reversibility by combined foulants is presented in Fig. 9. With the PA-TFC membrane both combined foulants caused significant decline in water flux over 10 h of operation for all conditions used (Fig. 8-a, b). In contrast the CTA membrane showed no flux decline over 10 h of operation in half of the cases. For the others a moderate reduction in water flux occurred with the normalized flux being 0.71 (above critical flux) and 0.8 (at critical flux) for alginate + colloidal silica, and 0.73 (above critical flux) for alginate + gypsum. The lower susceptibility of the CTA membrane to fouling is attributed, in part, to the relatively lower initial flux. Additionally the cleaning process depends on various factors such as the foulant-foulant

33

interaction and foulant-membrane interaction which is influenced by surface roughness, hydrophilicity and bonding to functional groups [60]. Regarding the CTA membrane, Liu et al. [8] reported that after combined fouling by alginate + gypsum the water flux only recovered to approximately 80%; their experiments were operated at a flux of 17.6 LMH (DS 4 M) with 20 Na_2SO_4 mM and 35 $CaCl_2$ mM. However, in the current study, with 20 Na_2SO_4 mM and 20 $CaCl_2$ mM (e.g., gypsum scaling)and at a lower flux of 9.0 LMH (DS 1 M) the CTA membrane exhibited a high water flux recovery of 93%. This shows that the initial flux and concentration of Ca^{2+} ions are critical in determining flux recovery for this combined foulant.

Another one, Kim et al. [27] observed that fouling reversibility with alginate + colloidal silica was only 93% compared to complete flux recovery (i.e., 100%) for single foulants. Their operations were at identical initial fluxes of 25.3 LMH (DS 5 M) with IS =50 mM and pH=7. Meanwhile, the current study indicated that full restoration of water flux was obtained when operating close to critical flux i.e. at 5.4 LMH (DS 0.5 M). From the results (Fig 9), the critical flux for reversibility for the CTA membrane could also be identified. A summary is given in Table 5.

Figure 9. Water flux recovery after physical cleaning of membranes fouled by various combined foulants: (a) alginate + colloidal silica, (b) alginate + gypsum scaling under operational critical flux (above critical flux, critical flux, below critical flux). Water permeating between 15 min and 30

644 min after the physical cleaning step is used for the calculation of flux recovery. Blanks exist where

645 no fouling was observed during the fouling tests.

646

647 As shown in Fig. 9-a, b the results for the PA-TFC membrane are significantly different with the

648 water flux declining after 10 h to normalized fluxes of *circa* 0.6. After combined fouling by alginate

649 + colloidal silica full reversibility was not exhibited with the water flux recovery being around 96%

650 at operation below the supposed critical flux i.e. at 8.3 LMH (DS 0.25 M) and approximately 92%

651 for operation at the supposed critical flux i.e. at 12.8 LMH (DS 0.5 M). For the other combined

652 foulants, 100% recovery was found at operation below critical flux values of 2.3 LMH (DS 0.15

653 M). For the PA-TFC membrane, the complete set of critical flux for reversibility is summarized in

654 Table 5.

655

656

657 **Table 5.** Critical flux values for fouling reversibility (LMH)

Foulants	Critical Flux for fouling reversibility (J_{ci})	
	CTA	PA-TFC
Single foulant		
Alginate	< 15.9	12.8
Colloidal silica	< 12.5	8.3
Gypsum	< 15.9	< 12.8
Combined foulants		
Alginate + gypsum	< 9.0	2.3
Alginate + colloidal silica	5.4	< 8.3

658 Note: The values above are specific for the FO membrane process with the conditions: i) FO mode

659 (AL-FS), ii) Feed and draw flow rate of 300 mL/min (equivalent CFV of 6.66 cm/s), iii) Foulant

660 concentration: 200 mg/L alginate, 1000 mg/L colloidal silica, gypsum scaling (20 mM Na_2SO_4 and

661 20 mM $CaCl_2$), and iv) determination after fouling for 10 h followed by evaluation of fouling

662 reversibility after a 30 min physical clean.

663

664 **4. Conclusions**

665 First, the existence of critical fluxes in an FO process (CTA and PA-TFC membranes with three

666 single separate foulants) was demonstrated through a reliable stepping method (DS concentration

667 stepping) in conjunction with water flux measurements in short-term experiments. The critical flux

668 behavior in the FO processes was evidently affected by the foulant type and the membrane type.

669 PA-TFC membrane outperformed the CTA membrane in terms of critical flux, which suggests that

670 the former might be favored for practical applications. The critical flux values determined by flux

671 stepping ranged from 5.4 to 20.5 LMH (dependent upon membrane-foulant combination) and these

672 would be adequate for applications in certain FO processes. Finally, 98-100% restoration of water

673 flux was achieved with the PA-TFC membrane at an operation either close to critical flux or below

674 critical flux (i.e., with negligible irreversible fouling), except for the combination of alginate and

675 colloidal silica. This study has confirmed that plant operation below the critical flux (which has

676 also been referred to as sustainable flux or sub-critical operation) is vital for the minimization of

677 chemical cleaning.

678

682 supported by an APEX award (AX170010) granted by a partnership between the Royal Society,

683 the British Academy and the Royal Academy of Engineering. This APEX award is for work on

684 Exploring Water Re-use – the Nexus of Politics, Technology and Economics.

685

686 **Appendix A: Supplementary data**

687

688 **References**

689

690 [1]   T.Y. Cath, A.E. Childress, M. Elimelech, Forward osmosis: Principles, applications, and

691   recent developments, J. Memb. Sci. 281 (2006) 70–87. doi:10.1016/j.memsci.2006.05.048.

692 [2]   C. Boo, M. Elimelech, S. Hong, Fouling control in a forward osmosis process integrating

693   seawater desalination and wastewater reclamation, J. Memb. Sci. (2013).

694   doi:10.1016/j.memsci.2013.05.004.

695 [3]   T.Y. Cath, N.T. Hancock, C.D. Lundin, C. Hoppe-Jones, J.E. Drewes, A multi-barrier

696   osmotic dilution process for simultaneous desalination and purification of impaired water,

697   J. Memb. Sci. (2010). doi:10.1016/j.memsci.2010.06.056.

698 [4]   M.M. Motsa, B.B. Mamba, A.R.D. Verliefde, Forward osmosis membrane performance

699   during simulated wastewater reclamation: Fouling mechanisms and fouling layer

700   properties, J. Water Process Eng. 23 (2018) 109–118. doi:10.1016/j.jwpe.2018.03.007.

701 [5]   F. Volpin, E. Fons, L. Chekli, J.E. Kim, A. Jang, H.K. Shon, Hybrid forward osmosis-

702   reverse osmosis for wastewater reuse and seawater desalination: Understanding the

703   optimal feed solution to minimise fouling, Process Saf. Environ. Prot. 117 (2018) 523–

704   532. doi:10.1016/j.psep.2018.05.006.

705 [6]   L. Chekli, S. Phuntsho, J.E. Kim, J. Kim, J.Y. Choi, J.S. Choi, S. Kim, J.H. Kim, S. Hong,

706   J. Sohn, H.K. Shon, A comprehensive review of hybrid forward osmosis systems:

707   Performance, applications and future prospects, J. Memb. Sci. (2016).

708   doi:10.1016/j.memsci.2015.09.041.

709 [7]   G. Blandin, A.R.D. Verliefde, J. Comas, I. Rodriguez-Roda, P. Le-Clech, Efficiently

710   combining water reuse and desalination through forward osmosis-reverse osmosis (FO-

711   RO) hybrids: A critical review, Membranes (Basel). (2016).

712   doi:10.3390/membranes6030037.

713 [8]   A.J. Ansari, F.I. Hai, W.E. Price, J.E. Drewes, L.D. Nghiem, Forward osmosis as a

714   platform for resource recovery from municipal wastewater - A critical assessment of the

715   literature, J. Memb. Sci. 529 (2017) 195–206. doi:10.1016/j.memsci.2017.01.054.

716 [9]   A.J. Ansari, F.I. Hai, W. Guo, H.H. Ngo, W.E. Price, L.D. Nghiem, Factors governing the

717   pre-concentration of wastewater using forward osmosis for subsequent resource recovery,

718   Sci. Total Environ. 566–567 (2016) 559–566. doi:10.1016/j.scitotenv.2016.05.139.

719 [10] Q. She, R. Wang, A.G. Fane, C.Y. Tang, Membrane fouling in osmotically driven

720   membrane processes: A review, J. Memb. Sci. 499 (2016) 201–233.

721   doi:10.1016/j.memsci.2015.10.040.

722 [11] M. Xie, J. Lee, L.D. Nghiem, M. Elimelech, Role of pressure in organic fouling in forward

723   osmosis and reverse osmosis, J. Memb. Sci. 493 (2015) 748–754.

724   doi:10.1016/j.memsci.2015.07.033.

725 [12] W.C.L. Lay, T.H. Chong, C.Y. Tang, A.G. Fane, J. Zhang, Y. Liu, Fouling propensity of

726   forward osmosis: Investigation of the slower flux decline phenomenon, Water Sci.

727   Technol. 61 (2010) 927–936. doi:10.2166/wst.2010.835.

728 [13] A.G. Fane, T.H. Chong, J. Zhang, W.C.L. Lay, The Effect of Flux and Pressure on Fouling

729   in Reverse Osmosis Desalination, Proceedings IDA World Congress, (2009) Paper DB09-

730   128.

731   [14]   Y. Liu, B. Mi, Combined fouling of forward osmosis membranes: Synergistic foulant

732   interaction and direct observation of fouling layer formation, J. Memb. Sci. 407–408

733   (2012) 136–144. doi:10.1016/j.memsci.2012.03.028.

734   [15]   R.W. Field, D. Wu, J.A. Howell, B.B. Gupta, Critical flux concept for microfiltration

735   fouling, J. Memb. Sci. 100 (1995) 259–272. doi:10.1016/0376-7388(94)00265-Z.

736   [16]   J.A. Howell, Sub-critical flux operation of microfiltration, J. Memb. Sci. 107 (1995) 165–

737   171. doi:10.1016/0376-7388(95)00114-R.

738   [17]   P. Bacchin, P. Aimar, V. Sanchez, Model for colloidal fouling of membranes, AIChE J. 41

739   (1995) 368–376. doi:10.1002/aic.690410218.

740   [18]   F. Wicaksana, A.G. Fane, P. Pongpairoj, R. Field, Microfiltration of algae (Chlorella

741   sorokiniana): Critical flux, fouling and transmission, J. Memb. Sci. 387–388 (2012) 83–92.

742   doi:10.1016/j.memsci.2011.10.013.

743   [19]   J. Xu, L.G. Ruan, X. Wang, Y.Y. Jiang, L.X. Gao, J.C. Gao, Ultrafiltration as pretreatment

744   of seawater desalination: Critical flux, rejection and resistance analysis, Sep. Purif.

745   Technol. 85 (2012) 45–53. doi:10.1016/j.seppur.2011.09.038.

746   [20]   L. Qi, X. Zheng, G. Li, Factors influencing critical flux of UF membrane in drinking water

747   treatment, Desalin. Water Treat. 56 (2015) 3305–3312.

748   doi:10.1080/19443994.2014.968879.

749   [21]   M. Stoller, Effective fouling inhibition by critical flux based optimization methods on a

750   NF membrane module for olive mill wastewater treatment, Chem. Eng. J. 168 (2011)

751   1140–1148. doi:10.1016/j.cej.2011.01.098.

752   [22]   Y. Lan, K. Groenen-Serrano, C. Coetsier, C. Causserand, Fouling control using critical,

753   threshold and limiting fluxes concepts for cross-flow NF of a complex matrix: Membrane

754   BioReactor effluent, J. Memb. Sci. 524 (2017) 288–298.

755   doi:10.1016/j.memsci.2016.11.001.

756   [23] T.H. Chong, F.S. Wong, A.G. Fane, Implications of critical flux and cake enhanced

757   osmotic pressure (CEOP) on colloidal fouling in reverse osmosis: Experimental

758   observations, J. Memb. Sci. 314 (2008) 101–111. doi:10.1016/j.memsci.2008.01.030.

759   [24] C.Y. Tang, Y.N. Kwon, J.O. Leckie, Fouling of reverse osmosis and nanofiltration

760   membranes by humic acid-Effects of solution composition and hydrodynamic conditions,

761   J. Memb. Sci. 290 (2007) 86–94. doi:10.1016/j.memsci.2006.12.017.

762   [25] R.W. Field, G.K. Pearce, Critical, sustainable and threshold fluxes for membrane filtration

763   with water industry applications, Adv. Colloid Interface Sci. 164 (2011) 38–44.

764   doi:10.1016/j.cis.2010.12.008.

765   [26] Y. Jang, H. Cho, Y. Shin, Y. Choi, S. Lee, J. Koo, Comparison of fouling propensity and

766   physical cleaning effect in forward osmosis, reverse osmosis, and membrane distillation,

767   Desalin. Water Treat. 3994 (2016) 1–10. doi:10.1080/19443994.2016.1152650.

768   [27] Y. Kim, M. Elimelech, H.K. Shon, S. Hong, Combined organic and colloidal fouling in

769   forward osmosis: Fouling reversibility and the role of applied pressure, J. Memb. Sci. 460

770   (2014) 206–212. doi:10.1016/j.memsci.2014.02.038.

771   [28] Y.N. Wang, E. Järvelä, J. Wei, M. Zhang, H. Kyllönen, R. Wang, C.Y. Tang, Gypsum

772   scaling and membrane integrity of osmotically driven membranes: The effect of membrane

773   materials and operating conditions, Desalination. 377 (2016) 1–10.

774   doi:10.1016/j.desal.2015.08.024.

775   [29] M. Elimelech, Gypsum Scaling and Cleaning in Forward Osmosis : Measurements and

776   Mechanisms, Environ. Sci. Technol. 44 (2010) 2022–2028.

777   [30] N.M. Mazlan, P. Marchetti, H.A. Maples, B. Gu, S. Karan, A. Bismarck, A.G. Livingston,

778   Organic fouling behaviour of structurally and chemically different forward osmosis

779   membranes: A study of cellulose triacetate and thin film composite membranes, J. Memb.

780   Sci. 520 (2016) 247–261. doi:10.1016/j.memsci.2016.07.065.

781   [31]   B. Mi, M. Elimelech, Organic fouling of forward osmosis membranes: Fouling

782   reversibility and cleaning without chemical reagents, J. Memb. Sci. 348 (2010) 337–345.

783   doi:10.1016/j.memsci.2009.11.021.

784   [32]   P. Bacchin, P. Aimar, R.W. Field, Critical and sustainable fluxes: Theory, experiments and

785   applications, J. Memb. Sci. 281 (2006) 42–69. doi:10.1016/j.memsci.2006.04.014.

786   [33]   S.P. Beier, G. Jonsson, Critical flux determination by flux-stepping, AIChE J. 56 (2010)

787   1739–1747. doi:10.1002/aic.

788   [34]   Y. Wang, F. Wicaksana, C.Y. Tang, A.G. Fane, Direct Microscopic Observation of

789   Forward Osmosis Membrane Fouling, Environ. Sci. Technol. 44 (2010) 7102–7109.

790   doi:10.1021/es101966m.

791   [35]   S. Zou, Y. Gu, D. Xiao, C.Y. Tang, The role of physical and chemical parameters on

792   forward osmosis membrane fouling during algae separation, J. Memb. Sci. 366 (2011)

793   356–362. doi:10.1016/j.memsci.2010.10.030.

794   [36]   G. Blandin, H. Vervoort, P. Le-Clech, A.R.D. Verliefde, Fouling and cleaning of high

795   permeability forward osmosis membranes, J. Water Process Eng. 9 (2016) 161–169.

796   doi:10.1016/j.jwpe.2015.12.007.

797   [37]   T.P.N. Nguyen, B.M. Jun, J.H. Lee, Y.N. Kwon, Comparison of integrally asymmetric and

798   thin film composite structures for a desirable fashion of forward osmosis membranes, J.

799   Memb. Sci. 495 (2015) 457–470. doi:10.1016/j.memsci.2015.05.039.

800   [38]   S.J. Kim, S. Kook, B.E. O'Rourke, J. Lee, M. Hwang, Y. Kobayashi, R. Suzuki, I.S. Kim,

801   Characterization of pore size distribution (PSD) in cellulose triacetate (CTA) and

802   polyamide (PA) thin active layers by positron annihilation lifetime spectroscopy (PALS)

803   and fractional rejection (FR) method, J. Memb. Sci. 527 (2017) 143–151.

804   doi:10.1016/j.memsci.2016.12.064.

805   [39]   J. Lee, S. Kook, C. Lee, I.S. Kim, Effect of intermittent pressure-assisted forward osmosis

806   (I-PAFO) on organic fouling, Desalination. 419 (2017) 60–69.

807   doi:10.1016/j.desal.2017.06.003.

808   [40]   N.Y. Yip, A. Tiraferri, W.A. Phillip, J.D. Schiffman, M. Elimelech, High Performance

809   Thin-Film Composite Forward Osmosis Membrane, Environ. Sci. Technol. (2010).

810   doi:10.1021/es1002555.

811   [41]   M.M. Motsa, B.B. Mamba, A.R.D. Verliefde, Combined colloidal and organic fouling of

812   FO membranes: The influence of foulant-foulant interactions and ionic strength, J. Memb.

813   Sci. 493 (2015) 539–548. doi:10.1016/j.memsci.2015.06.035.

814   [42]   C. Boo, S. Lee, M. Elimelech, Z. Meng, S. Hong, Colloidal fouling in forward osmosis:

815   Role of reverse salt diffusion, J. Memb. Sci. 390–391 (2012) 277–284.

816   doi:10.1016/j.memsci.2011.12.001.

817   [43]   S. Zou, Y.N. Wang, F. Wicaksana, T. Aung, P.C.Y. Wong, A.G. Fane, C.Y. Tang, Direct

818   microscopic observation of forward osmosis membrane fouling by microalgae: Critical

819   flux and the role of operational conditions, J. Memb. Sci. 436 (2013) 174–185.

820   doi:10.1016/j.memsci.2013.02.030.

821   [44]   C.Y. Tang, Q. She, W.C.L. Lay, R. Wang, A.G. Fane, Coupled effects of internal

822   concentration polarization and fouling on flux behavior of forward osmosis membranes

823   during humic acid filtration, J. Memb. Sci. 354 (2010) 123–133.

824   doi:10.1016/j.memsci.2010.02.059.

825   [45]   M.M. Motsa, B.B. Mamba, A. D'Haese, E.M.V. Hoek, A.R.D. Verliefde, Organic fouling

826   in forward osmosis membranes: The role of feed solution chemistry and membrane

827   structural properties, J. Memb. Sci. 460 (2014) 99–109.

828   doi:10.1016/j.memsci.2014.02.035.

829   [46] Q. She, X. Jin, Q. Li, C.Y. Tang, Relating reverse and forward solute diffusion to

830   membrane fouling in osmotically driven membrane processes, Water Res. 46 (2012)

831   2478–2486. doi:10.1016/j.watres.2012.02.024.

832   [47] W.S. Ang, M. Elimelech, Protein (BSA) fouling of reverse osmosis membranes:

833   Implications for wastewater reclamation, J. Memb. Sci. 296 (2007) 83–92.

834   doi:10.1016/j.memsci.2007.03.018.

835   [48] B. Mi, M. Elimelech, Chemical and physical aspects of organic fouling of forward osmosis

836   membranes, J. Memb. Sci. 320 (2008) 292–302. doi:10.1016/j.memsci.2008.04.036.

837   [49] Y. Gu, Y.N. Wang, J. Wei, C.Y. Tang, Organic fouling of thin-film composite polyamide

838   and cellulose triacetate forward osmosis membranes by oppositely charged

839   macromolecules, Water Res. 47 (2013) 1867–1874. doi:10.1016/j.watres.2013.01.008.

840   [50] C. Kim, S. Lee, S. Hong, Application of osmotic backwashing in forward osmosis:

841   Mechanisms and factors involved, Desalin. Water Treat. 43 (2012) 314–322.

842   doi:10.1080/19443994.2012.672215.

843   [51] M. Xie, S.R. Gray, Gypsum scaling in forward osmosis: Role of membrane surface

844   chemistry, J. Memb. Sci. 513 (2016) 250–259. doi:10.1016/j.memsci.2016.04.022.

845   [52] Y. Liu, B. Mi, Effects of organic macromolecular conditioning on gypsum scaling of

846   forward osmosis membranes, J. Memb. Sci. 450 (2014) 153–161.

847   doi:10.1016/j.memsci.2013.09.001.

848   [53] M. Xie, L.D. Nghiem, W.E. Price, M. Elimelech, Impact of organic and colloidal fouling

849   on trace organic contaminant rejection by forward osmosis: Role of initial permeate flux,

850   Desalination. 336 (2014) 146–152. doi:10.1016/j.desal.2013.12.037.

851   [54]   E. Arkhangelsky, F. Wicaksana, A.A. Al-Rabiah, S.M. Al-Zahrani, R. Wang,

852   Understanding the interaction between biomacromolecules and their influence on forward

853   osmosis process, Desalination. 385 (2016) 12–23. doi:10.1016/j.desal.2016.02.006.

854   [55]   B. Mi, M. Elimelech, Silica scaling and scaling reversibility in forward osmosis, DES. 312

855   (2013) 75–81. doi:10.1016/j.desal.2012.08.034.

856   [56]   A.S. Kim, E.M. V Hoek, Cake Structure in Dead-End Membrane Filtration: Monte Carlo

857   Simulations, Environ. Eng. Sci. 19 (2002) 373–386. doi:10.1089/109287502320963373.

858   [57]   J.C. Chen, M. Elimelech, A.S. Kim, Monte Carlo simulation of colloidal membrane

859   filtration: Model development with application to characterization of colloid phase

860   transition, J. Memb. Sci. 255 (2005) 291–305. doi:10.1016/j.memsci.2005.02.004.

861   [58]   S. Lee, C. Boo, M. Elimelech, S. Hong, Comparison of fouling behavior in forward

862   osmosis (FO) and reverse osmosis (RO), J. Memb. Sci. 365 (2010) 34–39.

863   doi:10.1016/j.memsci.2010.08.036.

864   [59]   M. Zhang, Q. She, X. Yan, C.Y. Tang, Effect of reverse solute diffusion on scaling in

865   forward osmosis: A new control strategy by tailoring draw solution chemistry,

866   Desalination. 401 (2017) 230–237. doi:10.1016/j.desal.2016.08.014.

867   [60]   E. Arkhangelsky, F. Wicaksana, C. Tang, A.A. Al-Rabiah, S.M. Al-Zahrani, R. Wang,

868   Combined organic-inorganic fouling of forward osmosis hollow fiber membranes, Water

869   Res. 46 (2012) 6329–6338. doi:10.1016/j.watres.2012.09.003.

870